Acta Crystallographica Section D
Biological Crystallography
ISSN 0907-4449

Structures of recombinant native and E202Q mutant human acetylcholinesterase complexed with the snake-venom toxin fasciculin-II

Gitay Kryger,[a] Michal Harel,[a] Kurt Giles,[a,b]† Lilly Toker,[b] Baruch Velan,[c] Arie Lazar,[c] Chanoch Kronman,[c] Dov Barak,[c] Naomi Ariel,[c] Avigdor Shafferman,[c] Israel Silman[b] and Joel L. Sussman[a]*

[a]Department of Structural Biology, Weizmann Institute of Science, Rehovot 76100, Israel, [b]Department of Neurobiology, Weizmann Institute of Science, Rehovot 76100, Israel, and [c]Biology Division, Israel Institute of Biological Research, Ness-Ziona 74100, Israel

† Present address: Department of Experimental Psychology, Oxford University, Oxford OX1 3UD, England.

Correspondence e-mail: joel.sussman@weizmann.ac.il

Received 5 April 2000
Accepted 28 July 2000

PDB References: acteylcholinesterase–fasciculin-II, 1b41; E202Q mutant acetylcholinesterase–fasciculin-II, 1f8u.

Structures of recombinant wild-type human acetylcholinesterase and of its E202Q mutant as complexes with fasciculin-II, a 'three-finger' polypeptide toxin purified from the venom of the eastern green mamba (*Dendroaspis angusticeps*), are reported. The structure of the complex of the wild-type enzyme was solved to 2.8 Å resolution by molecular replacement starting from the structure of the complex of *Torpedo californica* acetylcholinesterase with fasciculin-II and verified by starting from a similar complex with mouse acetylcholinesterase. The overall structure is surprisingly similar to that of the *T. californica* enzyme with fasciculin-II and, as expected, to that of the mouse acetylcholinesterase complex. The structure of the E202Q mutant complex was refined starting from the corresponding wild-type human acetylcholinesterase structure, using the 2.7 Å resolution data set collected. Comparison of the two structures shows that removal of the charged group from the protein core and its substitution by a neutral isosteric moiety does not disrupt the functional architecture of the active centre. One of the elements of this architecture is thought to be a hydrogen-bond network including residues Glu202, Glu450, Tyr133 and two bridging molecules of water, which is conserved in other vertebrate acetylcholinesterases as well as in the human enzyme. The present findings are consistent with the notion that the main role of this network is the proper positioning of the Glu202 carboxylate relative to the catalytic triad, thus defining its functional role in the interaction of acetylcholinesterase with substrates and inhibitors.

1. Introduction

Acetylcholinesterase (AChE; E.C. 3.1.1.7) is among the most efficient enzymes, with a turnover number of $>10^4$ s^{-1}. While the structural and mechanistic origin of its catalytic power and high reactivity toward organophosphorus inhibitors has been a subject of interest for several decades, only recently has it been possible to delineate the unique functional architecture of the AChE active centre. This has been performed primarily by X-ray crystallography (Bourne *et al.*, 1995, 1999; Harel *et al.*, 1995, 1996; Sussman *et al.*, 1991) together with kinetic studies utilizing wild-type and mutant enzymes (Ordentlich *et al.*, 1996; Radic *et al.*, 1992; Shafferman, Kronman *et al.*, 1992). Knowledge of the structural and functional properties of AChE, in particular those of human AChE (hAChE), is important for the design of anti-Alzheimer drugs (Enz *et al.*, 1993; Weinstock, 1995), for development of improved procedures for treatment of intoxication by nerve agents (Millard & Broomfield, 1995; Shafferman, Ordentlich, Barak, Kronman *et*

al., 1996) and for the design of safer and more effective insecticides by comparison with the three-dimensional structure of the insect enzyme (Harel *et al.*, 2000).

The X-ray structures of AChEs are characterized by a deep and narrow gorge which penetrates halfway into the enzyme, with the catalytic site about 4 Å from its base (Silman & Sussman, 2000). In addition to the catalytic triad residue Glu334(*327*),[1] two other acidic amino acids are located near the bottom of the gorge: Glu202(*199*), located next to the catalytic Ser203(*200*), and Glu450(*443*), ∼9 Å away. These two residues are a part of the hydrogen-bond network in the AChE active centre (Ordentlich *et al.*, 1993), which also includes Tyr133(*130*) and two bridging water molecules [waters 681 and 615 in *T. californica* AChE (*Tc*AChE); PDB code 2ace; Koellner *et al.*, 2000]. This network may aid in maintaining the functional architecture of the catalytic machinery by ensuring correct positioning of Glu202(*199*) with respect to the catalytic triad. It is commonly thought that removal of a charged residue from the core of a protein will result in a local structural perturbation (Hendsch *et al.*, 1996). However, the effects of the replacement of Glu202(*199*) by glutamine upon AChE catalysis (Malany *et al.*, 2000; Radic *et al.*, 1992; Shafferman, Velan *et al.*, 1992), phosphylation (Hosea *et al.*, 1996; Ordentlich *et al.*, 1996, 1999), carbamylation (Ariel *et al.*, 1998; Radic *et al.*, 1992) and aging (Masson *et al.*, 1997; Ordentlich *et al.*, 1993, 1999; Saxena *et al.*, 1993, 1998; Shafferman, Ordentlich, Barak, Stein *et al.*, 1996) could be better explained by removal of the carboxylate from the vicinity of the His447(*440*) imidazole than by more substantial reorganization at the active centre. To further examine this issue, we compared the X-ray structure of the wild-type hAChE with that of the E202Q mutant.

Vertebrate AChEs occur in several different molecular forms which differ in their number of subunits (Massoulié *et al.*, 1993). Recombinant hAChE is secreted into the culture medium as a mixture of monomers, dimers and tetramers (Velan *et al.*, 1991). Additional heterogeneity may arise from variations in the extent of glycosylation (Velan *et al.*, 1993) and owing to proteolytic 'nicking'. Such heterogeneity may severely impede crystallization. To partially alleviate this problem, mutants of the wild-type and the E202Q hAChEs were constructed in which the C terminus had been truncated so as to allow expression only of a monomeric form, as had already been performed to assist crystallization of recombinant mouse AChE (mAChE; Marchot *et al.*, 1996). Crystallization of the truncated hAChEs was further aided by complexation with fasciculin-II (FAS-II; Karlsson *et al.*, 1984), a 61 amino-acid polypeptide secreted in the venom of the eastern green mamba (*D. angusticeps*) which is a member of the 'three-finger' toxin family (Harvey, 1991). FAS-II binds tightly to AChE of higher vertebrates (Radic *et al.*, 1994) and had already been found to facilitate crystallization of both *Tc*AChE and mAChE. In both these structures, fasciculin interacts predominantly with the peripheral anionic site without affecting the structure of the active centre (Bourne *et al.*, 1995; Giles *et al.*, 1997; Harel *et al.*, 1995).

[1] Human numbering, with *T. californica* numbering (when required) in brackets (Massoulié *et al.*, 1992).

2. Experimental

2.1. Mutagenesis, generation and purification of truncated recombinant hAChE

Truncation of the C terminus of the T subunit of hAChE (Soreq *et al.*, 1990) was performed by DNA cassette replacement (Shafferman, Kronman *et al.*, 1992). Specifically, the 187 bp DNA fragment between *Bss*HII and *Sal*I in pL5CA (Kronman *et al.*, 1992) was replaced by the synthetic DNA duplex. The truncated DNA sequence was introduced into a tripartite expression vector also expressing the reporter gene *cat* and the selection marker *neo*. The expression vector coding for expression of monomeric hAChE was introduced into HEK 293 cells. Stable clones, secreting high levels (>4 U ml^{-1} h^{-1}) of truncated enzyme (ΔCter-hAChE), were isolated and used in large-scale production (Kronman *et al.*, 1992), thus yielding amounts of purified enzyme adequate for crystallization. A homologous truncated DNA sequence, in which site-directed mutagenesis afforded expression of the E202Q mutant (Shafferman, Velan *et al.*, 1992), was generated in order to study the importance of the negative charge next to the catalytic Ser203 in the active site. This mutant was

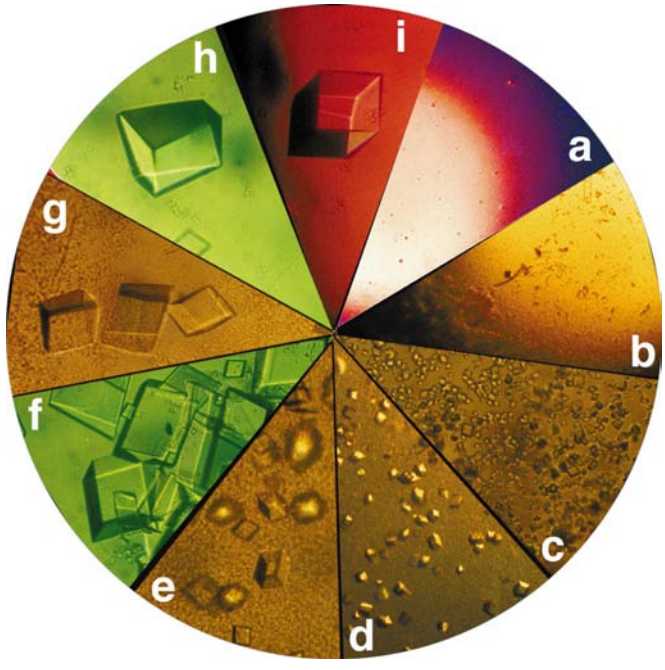

Figure 1
Incremental improvement in hAChE–FAS-II crystallization *via* optimization of conditions and repetitive recrystallization. (*a*) First appearance of crystals in the Hampton Screen I, condition No. 4 (0.1 *M* Tris–HCl pH 8.5, 2 *M* ammonium sulfate). (*b*) Reduction of ionic strength of protein stock solution (from 100 to 10 m*M* NaCl) and ammonium sulfate concentration lowered to 1.8 *M*. (*c*) 2:1 protein stock to precipitant in drop, ammonium sulfate concentration lowered to 1.6 *M*. (*d*) Using HEPES pH 7.0. (*e*) pH 7.2 and 1:1 protein stock-to-precipitant ratio. (*f*) pH 7.4 and 2:1 protein stock-to-precipitant ratio. (*g*) As (*e*) plus recrystallization. (*h*) As (*f*) plus recrystallization. (*i*) As (*f*) plus three cycles of recrystallization.

expressed and characterized similarly. Purification of both WT and E202Q hAChE was carried out by affinity chromatography as described previously (Sussman *et al.*, 1988).

Catalytic activity was assayed spectrophotometrically using acetylthiocholine (ATC) as a substrate by the Ellman method (Ellman *et al.*, 1961). Analytical sucrose density gradient centrifugation was performed on 5–20% sucrose gradients, as described previously (Velan *et al.*, 1991).

2.2. Crystallization and data collection

FAS-II was purchased from Alomone Labs (Jerusalem, Israel). Both WT hAChE and the E202Q mutant were co-crystallized as a stoichiometric complex with FAS-II. The pure and concentrated enzyme solution was combined with an aqueous solution of the toxin. In detail: 40 µl of hAChE (13–15 mg ml^{-1}) in 1 m*M* HEPES/10 m*M* NaCl/0.02% NaN_3 pH 7.0 were combined with 30 µl of FAS-II (2.3 mg ml^{-1}) in the same buffer to yield the protein stock solution. Ammonium sulfate at 1.4–1.8 *M* was adjusted to pH 7.5 with ammonium hydroxide and buffered with HEPES to pH 7.0–7.6 to form the well solution. The protein stock and the well solution were combined in 1:2, 1:1 and 2:1 ratios in 8 µl hanging drops. Crystals appeared within 1–2 d and grew over a period of three weeks (Fig. 1). These experiments yielded a shower of small (up to 100 µm) prism-shaped crystals with almost no optical activity, weak diffraction and high sensitivity to rotating-anode X-ray source radiation at 277 K. Nevertheless, rotating-anode data from these crystals were adequate for determining the unit-cell parameters (a = 149, b = 149, c = 247 Å, α = 90, β = 90, γ = 120°), lattice type (rhombohedral) and space group (*R*32). A recrystallization procedure was then applied to drops which had either given a shower of small crystals or had yielded a precipitate. This was performed by placing the drops over water overnight or until the precipitate and/or small crystals had dissolved and the drop had become clear; they were then placed over either the original reservoir or over a reservoir of lower precipitant concentration for recrystallization. This procedure usually produced fewer but larger crystals up to 800 µm in their longest dimension. These crystals were subsequently used for cryogenic data collection [using 20%(*w*/*v*) sucrose as a cryoprotectant] on a bending-magnet synchrotron X-ray source (X12-B/C at the National Synchrotron Light Source, Brookhaven National Laboratory). Under the conditions employed, the crystals diffracted to 2.7 Å. The data collected at the synchrotron confirmed the unit-cell parameters and space-group assignment and were used for structure determination (see Table 1).

Table 1
Data collection and processing.

Values for the highest resolution shell are given in parentheses.

	Native	E202Q
Space group	*R*32 (No. 155)	
No. of ASU in cell	18	
Unit-cell parameters (Å,°)	a = 149.0, b = 149.0, c = 247.0, α = 90.0, β = 90.0, γ = 120.0	a = 151.1, b = 151.1, c = 247.0, α = 90.0, β = 90.0, γ = 120.0
X-ray source	NSLS	
Beamline	X12C	
Wavelength (Å)	0.998	
Diffraction limit (Å)	2.8	2.7
No. of measured reflections	246782	270951
No. of unique reflections	26131	25075
Highest resolution shell (Å)	2.87–2.80	2.80–2.70
Completeness (%)	99.0 (97.3)	83.4 (20.6)
R_{sym} (on I) (%)	0.08 (0.47)	0.09 (0.24)
$I/\sigma(I)$	9.2 (4.2)	9.4 (2.6)

2.3. Structure determination and refinement

For crystal, data collection and processing information, see Table 1. The structures of the *Tc*AChE–FAS-II complex (Harel *et al.*, 1995; PDB code 1fss) and the mAChE–FAS-II complex (Bourne *et al.*, 1995; PDB code 1mah) were employed in parallel as probe models for the molecular-replacement procedure using the program *AMoRe* (Navaza, 1994) and

Figure 2
Alignment of the amino-acid sequences of hAChE, mAChE and *Tc*AChE. hAChE (Soreq *et al.*, 1990), mAChE (Rachinsky *et al.*, 1990) and *Tc*AChE (Schumacher *et al.*, 1986) were aligned using *CLUSTAL_X*, utilizing the secondary-structure option of this software to improve the alignment (Thompson *et al.*, 1997). Arrows denote β-strands and cylinders denote α-helices. Asterisks denote identity, colons show high similarity and full stops show moderate similarity.

subsequently as starting models for refinement. The amino-acid sequences of *Tc*AChE, mAChE and hAChE are very similar (Fig. 2); thus, the human structure could be assumed to be similar enough to both the *T. californica* and the mouse structures for either to be used in molecular replacement. The first and second solutions using each probe were related by one of the crystallographic symmetry operations of space group *R*32. The next best solution for each probe had a significantly poorer fit (see Table 2). Both models were refined separately using annealing and omit-map techniques. When refinement starting from either *Tc*AChE or mAChE converged to practically identical models, further refinement was pursued only from the model derived from the *Tc*AChE structure. Diffraction data for the E202Q mutant were refined similarly, but using the hAChE–FAS-II structure as the starting model. The structures were refined using *X-PLOR*, simulated annealing (Brünger, 1988) and *CNS* simulated annealing coupled with maximum likelihood (Adams *et al.*, 1997).

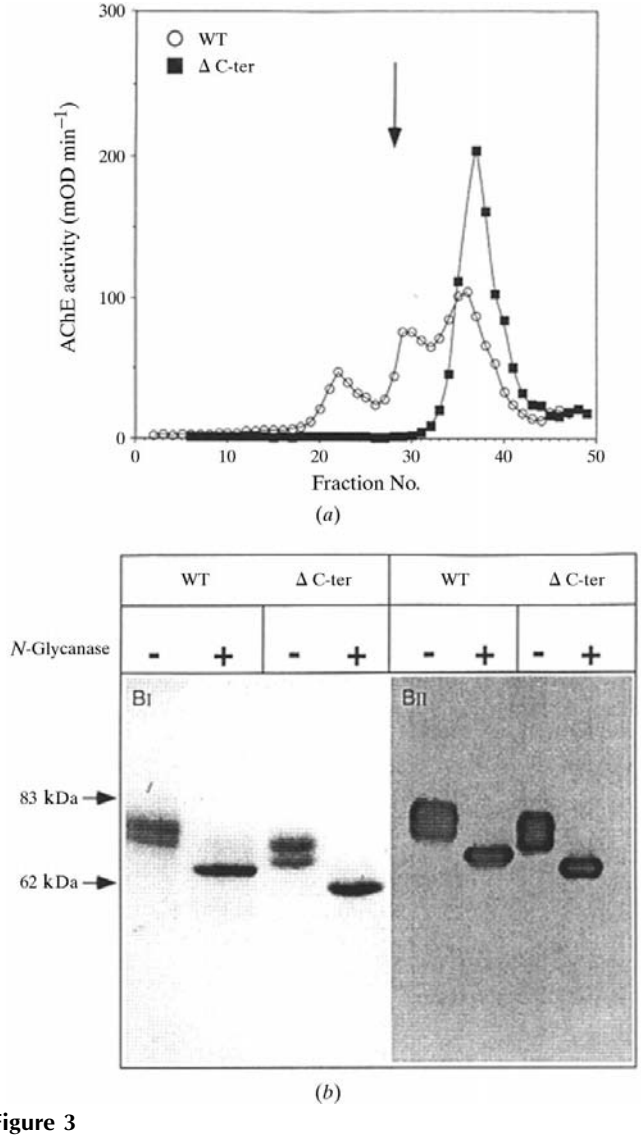

Figure 3
Characterization of recombinant hAChE. (*a*) Sucrose-density gradient; (*b*) SDS–PAGE gel of glycanase-treated and control hAChE [from left to right: Coomassie blue and anti-AChE antibody stains. The arrow denotes sedimentation of alkaline phosphatase (6.15)].

Table 2
Molecular replacement and first refinement cycle.

Probe model	*Tc*AChE–FAS-II (PDB code 1fss)	mAChE–FAS-II (PDB code 1mah)
Data resolution (Å)	30–4.0	30–4.0
Sequence identity, similarity to hAChE (%)	53, 72	88, 92
Correlation coefficient of top (next best) solution† (%)	47.7 (28.3)	60.3 (19.7)
R factor of top (next best) solution† (%)	45.8 (57.0)	41.4 (58.1)
R/R_{free} initial‡ (%)	43.8/45.0	38.5/39.3
R/R_{free} rigid§ (%)	443.2/45.3	336.9/37.5
R/R_{free} annealing¶ (%)	27.7/39.7	25.8/36.1

† *AMoRe*. ‡ *CNS*. § Group 1 = AChE, group 2 = FAS-II. ¶ 2000 K.

3. Results and discussion

3.1. Characterization of ΔCter-hAChE

The T subunit expressed was devoid of the C-terminal hydrophobic sequence corresponding to residues 544–583, including C580, which forms the interchain disulfide in oligomeric forms (Giles, 1997; Velan *et al.*, 1991). These residues were replaced by the pentapeptide ASEAP, which is part of the mature natural C-terminal sequence in the H subunit (Massoulié *et al.*, 1993). As expected, the resulting truncated enzyme displays the following structural and catalytic characteristics. (i) Sucrose-gradient centrifugation reveals a unique monomeric form, which sediments slightly more slowly than the monomer of the WT enzyme (Fig. 3). (ii) SDS–PAGE suggests that a similar degree of glycosylation-related microheterogeneity (Velan *et al.*, 1993) is present in both the WT and the truncated enzyme (Fig. 3). (iii) The molecular weight of the truncated polypeptide, after removal of sugar side chains by glycanase, is 60 kDa, compared with 64 kDa for the WT polypeptide as expected. (iv) The catalytic characteristics of the truncated enzyme, as well as the inhibition constants for its inhibition by an active-centre inhibitor such as edrophonium, by a peripheral site ligand such as propidium or by the inhibitor BW284C51, which spans both sites, are essentially identical to those reported for the WT enzyme (Shafferman, Velan *et al.*, 1992).

3.2. X-ray data and structure solution and refinement

A general concern in molecular replacement, the structure-elucidation method used for solving the mAChE and hAChE structures, is the introduction of model bias that may decrease the differences between the source and the target model during refinement. To address this problem, we solved the structure twice, using either *Tc*AChE–FAS-II or mAChE–FAS-II as the starting model. The fact that the refinements starting from either of these two models converged to a virtually identical structure (Table 3) indicated that we had

Table 3
Comparison of AChEs in AChE/FAS-II complexes: sequence identities and three-dimensional structures.

Sequence identity (%), upper right elements of the table; RMS deviation of C^{α} atoms coordinates (Å), lower left elements of the table.

	hAChE	mAChE	*Tc*AChE
hAChE	—	87	53
mAChE	0.7	—	54
*Tc*AChE	1.3	1.2	—

Table 4
Refinement and model statistics.

	Native	E202Q
Resolution range (Å)	30.0–2.8	40–2.9
No. of reflections	25997	22804
R factor (%)		
Work	19.0	17.0
Free	25.5	23.0
No. of atoms		
Protein (543 + 61 residues)	4581	4579
Hetero (carbohydrate, solvent)	38, 390	42, 203
Average *B* factors		
Protein	50.45	54.66
AChE	49.33	53.63
FAS-II	60.37	63.83
Water	50.87	50.16
Carbohydrate	75.37	96.03
RMSD from ideal values		
Bond length (Å)	0.010	0.010
Bond angle (°)	1.7	1.7
Dihedral angles (°)	23.9	23.9
Improper torsion angles (°)	1.23	1.24
Estimated coordinate error		
Low-resolution cutoff (Å)	5.00	6.00
E.s.d. from Luzzati plot (Å)	0.30	0.28
E.s.d. from σ_A (Å)	0.53	0.44

produced a *bona fide* unbiased model for hAChE. The quality of the refinement for both the wild-type and the E202Q hAChE–FAS-II complexes is shown in Table 4.

The electron density shows residues 5–490 and 497–543 of the hAChE polypeptide chain and all 61 residues of FAS-II. The 491–496 sequence, which lacks electron density, is homologous to the external 485–490 loop in *Tc*AChE, which is not seen in the native structure (PDB code 2ace), although it was discerned in the recently refined complex with E2020 (Kryger *et al.*, 1999; PDB code 1eve). In the mouse–FAS-II structure (PDB code 1mah) solved at 3.2 Å resolution, residues 4–543 have all been traced but, judging from their high temperature factors, residues 491–499 are poorly determined. The electron density of the WT hAChE structure shows the location of 390 solvent molecules and of one N-glycosylation site at N350.

3.3. Formation of the physiological dimer is independent of crystal packing

*Tc*AChE–FAS-II, mAChE–FAS-II and hAChE–FAS-II pack very differently in their respective crystal structures (Fig. 4). Their solvent contents vary from 52% for *Tc*AChE–FAS-II through 64% for mAChE–FAS-II to 69% for hAChE–FAS-II. These differences are obviously a consequence of differences in molecular contacts between symmetry-related molecules. It is interesting to note, however, that although the hAChE–FAS-II complex shows the most extensive contacts between symmetry-related FAS-II molecules of the three, it shows the loosest overall packing of the AChE–FAS-II complex. Nevertheless, both the three-dimensional structures and the mode of association of the monomers to form the physiological dimer are essentially identical.

Table 5
Comparison of the quaternary structures of AChE dimers.

Distances (in Å) between pairs of C^{α} atoms of residue 58(*56*), chosen as one of the most distal residues from the four-helix bundle, of the symmetry-related molecule in the physiological dimer. The values in the table were calculated by first overlaying all four AChE monomer structures by a least-squares fit of the C^{α} atoms of their residues and then generating the second monomer of each dimer by a twofold symmetry operation. Distances were then measured between pairs of C^{α} atoms of residue 58(*56*) in the symmetry-related monomers.

	hAChE–FAS-II	mAChE–FAS-II	*Tc*AChE–FAS-II	*Tc*AChE
hAChE–FAS-II	—	9.5	5.1	7.5
mAChE–FAS-II	—	—	5.8	3.6
*Tc*AChE–FAS-II	—	—	—	3.0

AChE has an intrinsic tendency to dimerize through a four-helix bundle interface, which is reinforced by a disulfide bridge between the monomers (Giles, 1997). *Tc*AChE purified from the electric organ of *T. californica* is a homodimer, with a disulfide bridge linking the Cys537 residues of the two monomers. The dimer is found, as expected, in every crystal form characterized for *Tc*AChE, as well as in the *Tc*AChE–FAS-II structure. The human WT and mutant enzymes and mAChE are recombinant proteins expressed as monomers (see §2.1), which also migrate as monomers upon sucrose-gradient centrifugation. The ability to express a pure monomer rather than a mixture of monomers, dimers and tetramers was crucial to the crystallization of both mAChE and hAChE. However, at the high protein concentrations used for crystallization, the monomers, each one complexed with a FAS-II molecule, associated *via* the same four-helix bundle as seen in the *Tc*AChE dimer to form dimers of the complex rather than associating in alternative ways.

Close inspection and comparison of the dimer interface, which contains a four-helix bundle (helices 383–372 and 526–543), in all four crystal forms published so far for AChE reveals an unexpectedly large degree of flexibility in and out of the plane defined by the twofold axis normal to the four-helix bundle (see Table 5). This shows that this dimer interface is readily perturbed by crystal contacts and suggests that its flexibility may be of biological significance.

Indeed, when overlaying the second molecule from all four crystal forms published so far for AChE, it becomes visibly clear that the dimerization interface varies significantly not only between different species but also between the free and FAS-II bound *Tc*AChE crystal structures. Cys537 in *Tc*AChE, which is missing in the human and mouse structures owing to

deliberate truncation at the gene-construct level, forms a disulfide bond with its counterpart in the second member of the homodimer. Thus, the four-helix bundle interaction is too weak to maintain the dimer in solution, the covalent disulfide bridge being required to form a stable homodimer.

3.4. Comparison of the three-dimensional structures of the FAS-II complexes of hAChE, mAChE and *Tc*AChE

Close inspection of the hAChE–FAS-II structure reveals a high degree of similarity between it and the two other AChE–FAS-II complexes, *viz*. *Tc*AChE–FAS-II (Harel *et al.*, 1995) and mAChE–FAS-II (Bourne *et al.*, 1995), especially with respect to the active-site gorge. This is not surprising, considering the high degree of sequence identity between hAChE and both mAChE (87%) and *Tc*AChE (53%) (see Fig. 2 and Table 3). Small variations can be found in some loops and in the insertion/deletion regions. Our results validate the use of *Tc*AChE as a model for gaining a general understanding of the structures of vertebrate AChEs, but also open the way to the study of subtle differences in structure which may account for species-dependent differences in specificity for substrates and inhibitors (see, for example, Kraut *et al.*, 2000).

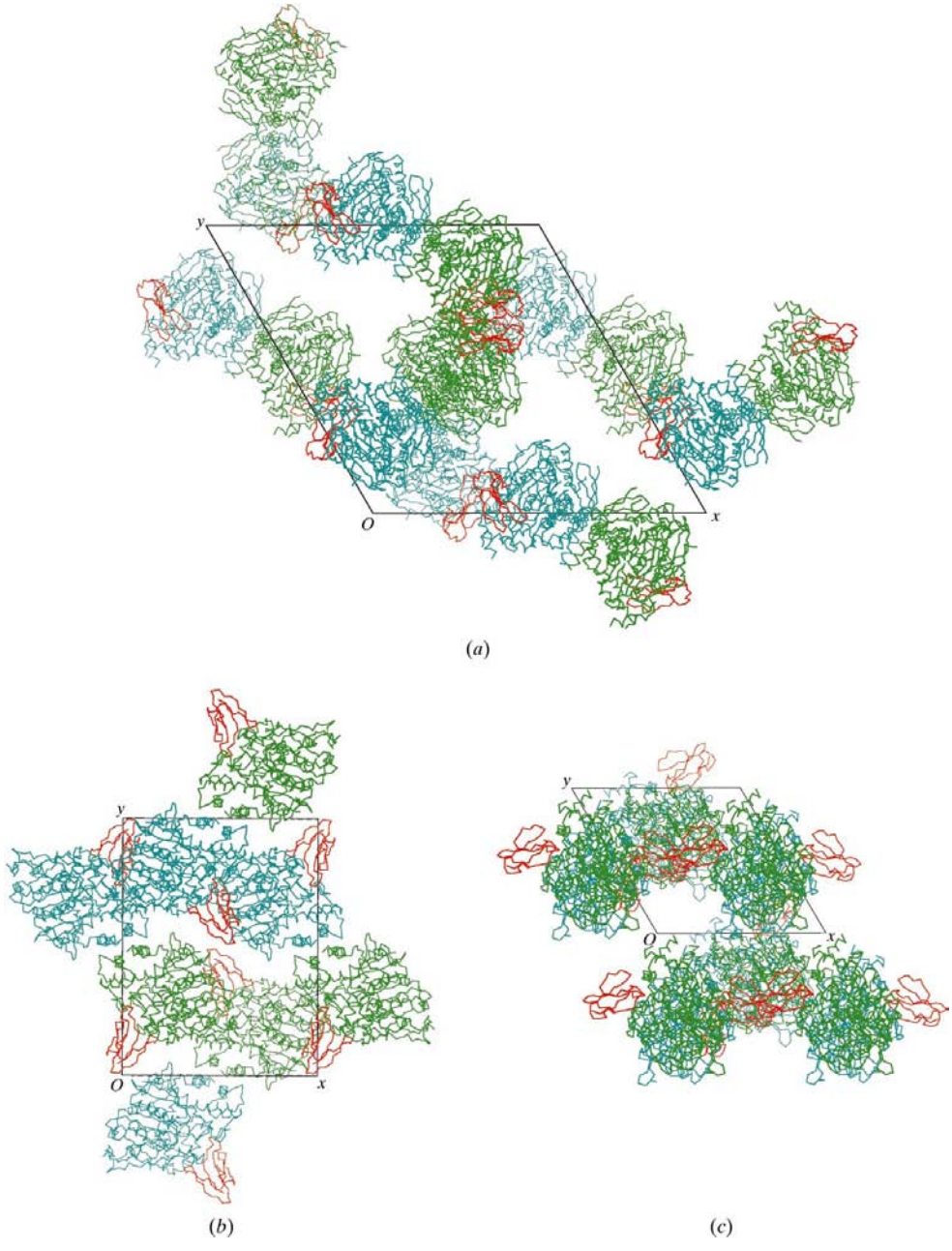

Figure 4
Schematic comparison of packing diagrams of AChE–FAS-II complexes, looking down the *z* axis with the monomers of the AChE dimers shown in green and blue and FAS-II shown in red: (*a*) hAChE–FAS-II; (*b*) *Tc*AChE–FAS-II; (*c*) mAChE–FAS-II.

The FAS-II molecule in the three complexes overlaps very well, with RMS values for C^{α} atoms of 0.55, 0.59 and 0.65 Å in the FAS-II complexes of hAChE *versus* mAChE, mAChE *versus* *Tc*AChE and hAChE *versus* *Tc*AChE, respectively. One of the most noticeable differences between the three structures is seen in the 319(*312*)–324(*317*) loop of the enzyme, where the backbones of the two mammalian main chains do not overlap with that of *Tc*AChE or the *Tc*AChE–FAS-II complex. Overall, the RMS of C^{α} atom positions between hAChE and *Tc*AChE is 1.3 Å, but for these six C^{α} atoms it is 5 Å, while it is only 0.7 Å between hAChE and mAChE, the same RMS value as for the entire lengths of these two mammalian sequences (Figs. 2 and 5; Table 3). In all three cases the loop is not involved in crystal contacts. It is interesting to note that the recently determined structure of the native mouse enzyme (Bourne *et al.*, 1999) does, however, overlap well in this region with the two mammalian/FAS-II complexes, the RMS deviation for chain *A* of the mouse structure for this region being 0.8 Å (overall 0.9 Å), 0.7 Å (overall 0.7 Å) and 4.1 Å (overall 1.3 Å) for the human–FAS-II, mouse–FAS-II and *Tc*AChE–FAS-II complexes, respectively. Thus, the difference in observed conformation for this region seems to reflect a real

difference between the mammalian and *T. californica* enzymes.

Conservation of the amino-acid residues lining the active-site gorge is very high: 26 residues are identical, two are similar, *viz*. Thr83(*Ser81*) and Tyr337(*Phe330*), and only two residues, both at the mouth of the gorge, are different in hAChE and mAChE *versus* *Tc*AChE, *viz*. Thr75(*Glu73*) and Leu76(*Gln74*) (Fig. 6).

3.5. Comparison of the FAS-II–AChE interaction for the three complexes

Fig. 7 depicts the contact surface between hAChE and FAS. The inhibitor is rotated 180° around the vertical axis to expose its contact with the enzyme. The distance criterion chosen to define contact between atoms in FAS-II and hAChE is 4 Å. The 'footprint' which FAS-II leaves on hAChE is coloured red and the reciprocal 'footprint' on FAS-II is coloured blue. This presentation shows how extensive the binding is. The gorge is efficiently sealed off from the 'outside' by the multiple contacts around its rim. Examining the list of atoms participating in the enzyme–inhibitor interface (Bourne *et al.*, 1995; Harel *et al.*, 1995) does not reveal significant differences between the three complexes. Overlaying the C^{α} atoms of the three enzymes reveals a small tilt of the toxin with respect to the enzyme between the three (Fig. 8). It is not clear if this small difference is a direct consequence of the interaction of the toxin with different enzymes or whether it is caused by different modes of crystal packing (see above).

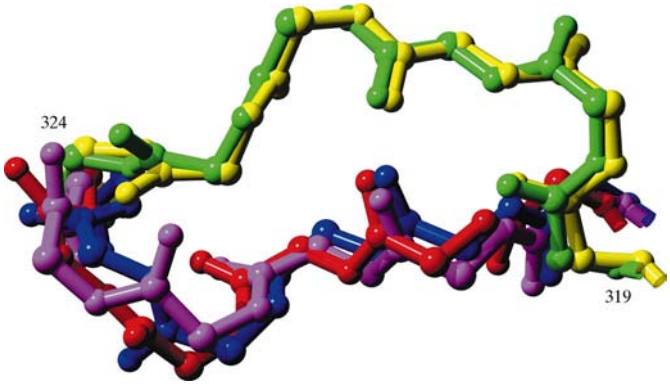

Figure 5
Overlay of the loop 319(*310*)–324(*317*) in three AChE–FAS-II complexes and two AChE apo structures: magenta, hAChE–FAS-II; red, mAChE–FAS-II; blue, mAChE (chain *A*); yellow, *Tc*AChE–FAS-II; green, *Tc*AChE.

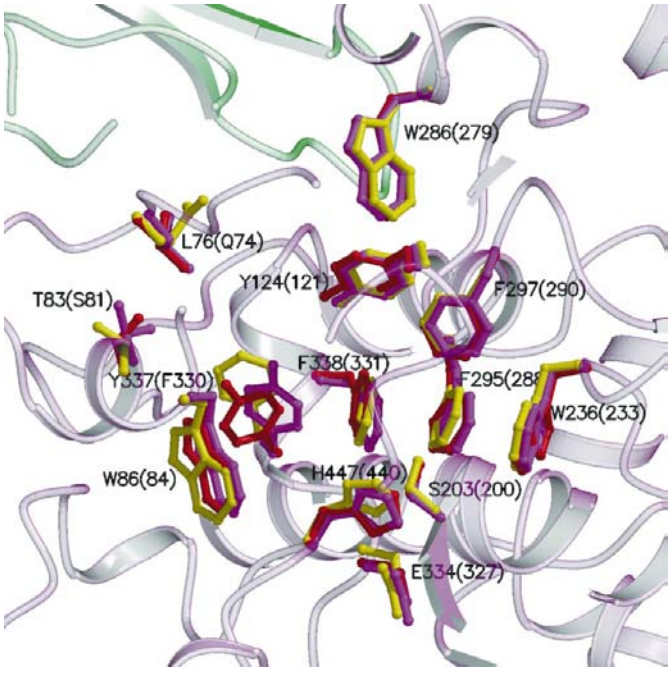

Figure 6
Comparison of the key residues within the active-site gorge in the three complex structures: magenta, hAChE–FAS-II; red, mAChE–FAS-II; yellow, *Tc*AChE–FAS-II. The grey ribbon denotes the hAChE backbone and the green ribbon the FAS-II backbone.

3.6. Comparison of the E202(*199*)Q mutant with the wild-type enzyme – importance of the hydrogen-bond network

The structure of the E202Q mutant was refined starting from the hAChE structure. Since, apart from their active centres, the two structures should be almost identical, the resulting RMS value (0.28 Å) for C^{α} atoms is not surprising. However, the observation that the respective active-site regions of the two enzymes overlap so well is both quite surprising and significant to our understanding of the functional architecture of AChE (Fig. 9). Residue Glu202(*199*), which is adjacent to the active-site gorge Ser203(*200*), is one of only three acidic residues at the bottom of the active-site gorge [the other two are the catalytic triad residue

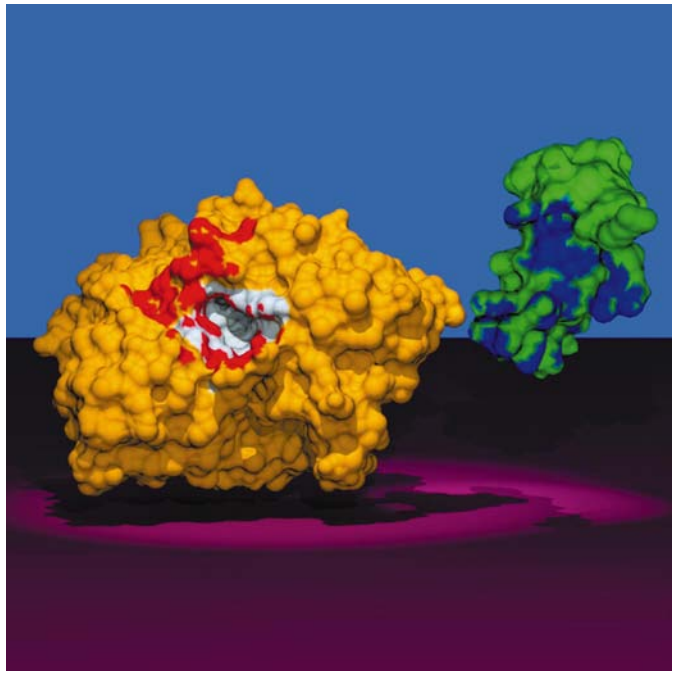

Figure 7
4.0 Å contact footprint between AChE and FAS-II. On the left, molecular surface of hAChE in yellow, with atoms $\leq$ 4.0 Å from FAS-II rendered in red and atoms lining the active-site gorge rendered in grey. On the right, molecular surface of FAS-II in green, with atoms $\leq$ 4.0 Å from hAChE atoms rendered in blue.

Glu334(*327*) and Glu450(*443*)] and is assumed to play an important role in AChE reactivity (Radic *et al.*, 1992; Shafferman, Velan *et al.*, 1992). Substitution of Glu202(*199*) by either a neutral (Ala, Gln) or an acidic (Asp) residue resulted in a tenfold to 100-fold decrease in the apparent bimolecular rates of hydrolysis of both the cationic substrate ATC and its neutral isoster 3,3-dimethylbutyl thioacetate (TB; Shafferman *et al.*, 1995; Shafferman, Velan *et al.*, 1992). This suggests that Glu202(*199*) participates mainly in the acylation step, rather than in substrate trafficking and accommodation. This reduction in catalytic efficiency, as well as the marked concomitant decreases in rates of carbamylation (∼10- to 50-fold; Ariel *et al.*, 1998; Radic *et al.*, 1992) and of phosphylation and ageing (∼10- to 100-fold; Hosea *et al.*, 1996; Masson *et al.*, 1997; Ordentlich *et al.*, 1993, 1996; Saxena *et al.*, 1998; Shafferman, Ordentlich, Barak, Stein *et al.*, 1996; Shafferman, Velan *et al.*, 1992), was rationalized in terms of interaction of residue Glu202(*199*) with the catalytic triad residue His447(*440*) (Shafferman, Ordentlich, Barak, Stein *et al.*, 1996). We proposed earlier that the precise positioning of the Glu202(*199*) carboxylate with respect to the His447(*440*) imidazole moieties is maintained by a network of hydrogen bonds that spans the cross-section of the active-site gorge (Ordentlich *et al.*, 1993). The main function of the hydrogen-bond network is to position the Glu202(*199*) carboxylate for optimal interaction with the catalytic triad (see Fig. 10). This network includes residues Glu450(*443*) and Tyr133(*130*), as well as two bridging water molecules corresponding to waters 615 and 681 in *Tc*AChE (PDB code 2ace). Apart from its role in positioning residue Glu202(*199*), the network is thought to participate in stabilization of the overall architecture of the AChE active centre, since replacement of either Glu202(*199*) or Glu450(*443*) seems to affect the accommodation of both charged and non-charged ligands (Shafferman *et al.*, 1998). In addition, substitution at position 202(*199*) by glutamine has a smaller effect on the affinity toward these ligands than the corresponding substitution by alanine. This difference between these two neutral substitutions has been ascribed to the capacity of glutamine but not of alanine to maintain the hydrogen-bond network. The structure of the E202Q enzyme is compatible with this notion, since the amide moiety of glutamine participates in a hydrogen-bond network analogous to that observed in the wild-type enzyme.

The finding that removal of the acidic residue from position 202(*199*) does not significantly perturb the architecture of the active centre is consistent also with the role assigned to Glu202(*199*) in the ageing of phosphylated AChEs (Shafferman, Ordentlich, Barak, Stein *et al.*, 1996). In the ageing process, the Glu202(*199*) carboxylate is thought to participate directly in stabilization of an intermediate. Substitutions at position 202(*199*) by either a neutral or an acidic residue should, therefore, affect the rates of ageing similarly (Ordentlich *et al.*, 1999; Shafferman, Ordentlich, Barak, Stein *et al.*, 1996). Thus, comparison of the structures of the wild-type and the E202Q hAChEs corroborates our previous conclusions regarding the functions of the hydrogen-bond network in the AChE active centre and the unique role of Glu202(*199*) in interaction with His447(*440*). In fact, a tripartite array, Glu334(*327*)–His447(*440*)–Glu202(*199*), was

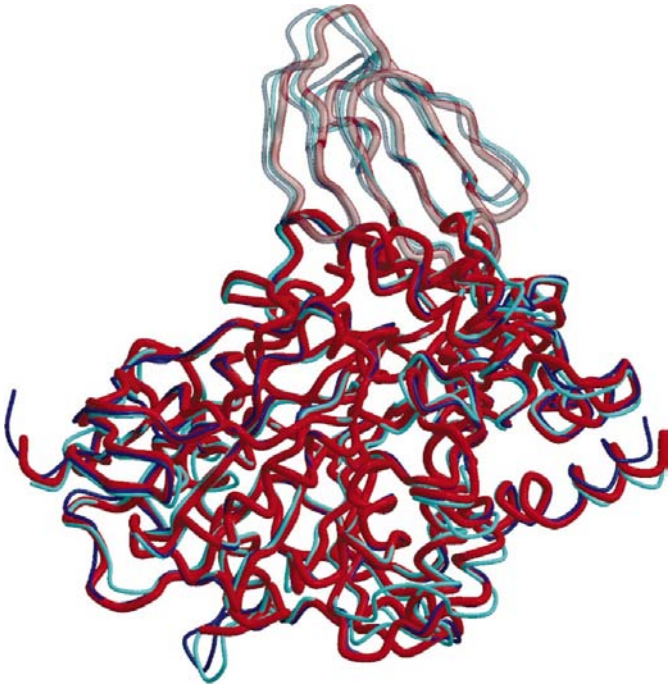

Figure 8
Overlay of three AChE–FAS-II complexes. Overlaying the C^{α} atoms of the three enzymes reveals the toxin to be bound at a slightly different angle in each case. hAChE in red, mAChE in blue and *Tc*AChE in cyan.

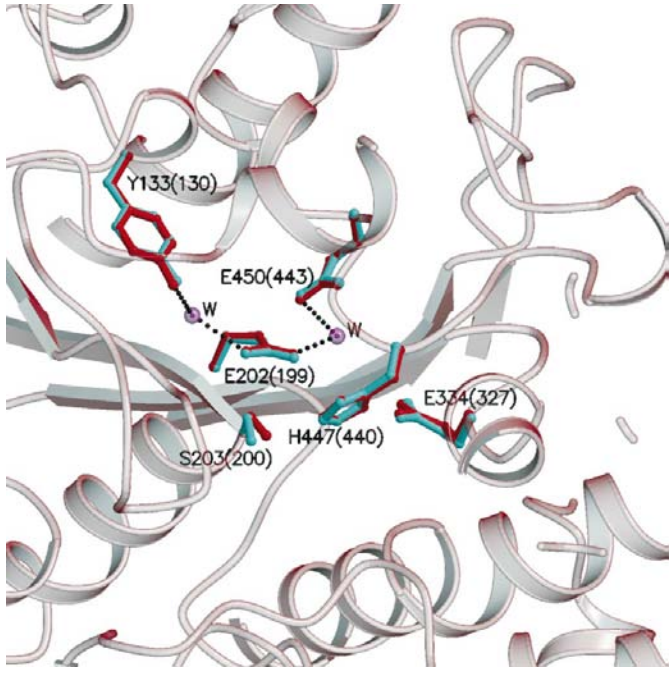

Figure 9
Comparison of WT hAChE *versus* the E202Q mutant: WT in magenta and E202Q mutant in cyan. W denotes water molecules. Note that the hydrogen-bond network [Tyr133(*130*)–Wat–Glu202(*199*)–Wat–Glu450(*443*)] is maintained in both the WT and mutant enzymes. The grey ribbon denotes the hAChE backbone.

recently proposed as a structural device for orienting the imidazole according to the steric and electrostatic features of the ligand bound to Ser203(*199*) (Millard *et al.*, 1999).

3.7. Conservation of water sites in AChE

The presence of a network of hydrogen-bonded waters in hAChE was originally deduced from model building and by analogy to the corresponding water network in the structure of *Tc*AChE (Ordentlich *et al.*, 1993). Our experimental confirmation of this water network in the WT hAChE structure, as well as in that of the E202Q mutant, strengthens the case for its involvement in the functional architecture of the different AChEs. It is also an example of the striking conservation of the positions of individual waters in homologous AChE structures. In general, many of the active-site and gorge buried water molecules, as well as surface water molecules, occupy the same positions in hAChE and *Tc*AChE. Following the finding of marked conservation of solvent-molecule positions in a set of *Tc*AChE crystal structures, which included the native enzyme and its complexes with various inhibitors (Koellner *et al.*, 2000), the present finding is a further manifestation of the importance of water molecules in the active-site gorge to the activity of AChE. This is a significant result considering the differences between the two enzymes, which include differences in sequence, in the source of the enzyme (recombinant product *versus* natural enzyme), crystallization conditions (*viz*. pH, ionic strength and composition) and space group. As mentioned by Koellner *et al.* (2000), we believe this conservation points to the importance of water for the definition of AChE in terms of folding and activity, a feature most likely to be shared by most proteins of this size.

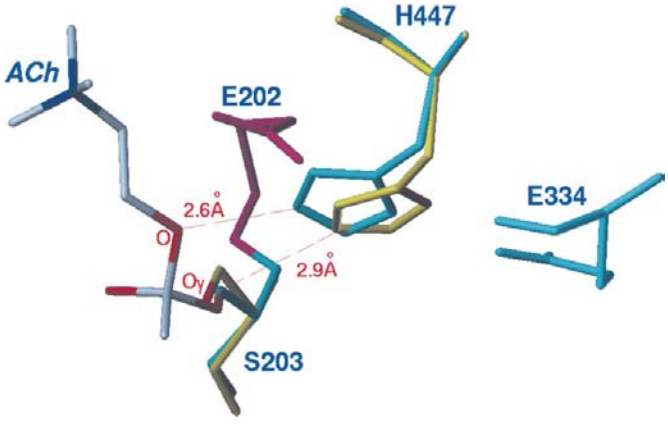

Figure 10
Model for the interaction between Glu202(*199*) and alternate positions of the catalytic His447(*440*) in substrate hydrolysis. The model of the tetrahedral hAChE–ACh intermediate is based on the X-ray structure of the transition-state analogue TMTFA with *Tc*AChE (Harel *et al.*, 1996) and on a previously described model for the involvement of the hydrogen-bond network in catalysis, phosphylation and in ageing (Shafferman *et al.*, 1998; Shafferman, Ordentlich, Barak, Kronman *et al.*, 1996). During acylation His447(*440*) can alternate between two positions. (*a*) The imidazole participates in proton abstraction from O^{γ} of the catalytic Ser203(*200*) [$N^{\varepsilon 2}$ is proximal, 2.9 Å away from Ser203(*200*) O^{γ}]. [In this orientation both His447(*440*) and Ser203(*200*) are shown in yellow.] (*b*) Transition of the tetrahedral intermediate into the acyl enzyme is assisted by proton transfer from the imidazolium to the choline oxygen, followed by release of the choline moiety ($N^{\varepsilon 2}$ is 2.6 Å from the choline oxygen). [In this orientation both His447(*440*) and Ser203(*200*) are shown in light blue.] Stabilization of the His447(*440*) imidazolium in the two alternate positions is facilitated by interactions with the carboxylate of Glu202(*199*) (Glu202 $O^{\varepsilon 1}$ is 3.08–3.23 Å from the centroid of the imidazolium ring).

This work was supported by the US Army Medical Research Acquisition Activity under Contract Nos. DAMD17-96-C-6088 and DAMD17-00-C-0021 to AS, and DAMD17-97–2-7022 to JLS and IS, the European Union IVth Framework in Biotechnology, the Kimmelman Center for Biomolecular Structure and Assembly, Rehovot, Israel, the Nella and Leon Benoziyo Center for Neurosciences and the Dana Foundation. IS is Bernstein–Mason Professor of Neurochemistry. We thank Professor Hermona Soreq for generously providing the original DNA clone expressing hAChE.

References

Adams, P. D., Pannu, N. S., Read, R. J. & Brünger, A. T. (1997). *Proc. Natl Acad. Sci. USA*, **94**, 5018–5023.
Ariel, N., Ordentlich, A., Barak, D., Bino, T., Velan, B. & Shafferman, A. (1998). *Biochem. J.* **335**, 95–102.
Bourne, Y., Taylor, P., Bougis, P. E. & Marchot, P. (1999). *J. Biol. Chem.* **274**, 2963–2970.
Bourne, Y., Taylor, P. & Marchot, P. (1995). *Cell*, **83**, 503–512.
Brünger, A. T. (1988). *J. Mol. Biol.* **203**, 803–816.
Ellman, G. L., Courtney, K. D., Andres, V. & Featherstone, R. M. (1961). *Biochem. Pharmacol.* **7**, 88–95.
Enz, A., Amstutz, R., Boddeke, H., Gmelin, G. & Malanowski, J. (1993). *Prog. Brain Res.* **98**, 431–438.
Giles, K. (1997). *Protein Eng.* **10**, 677–685.
Giles, K., Raves, M. L., Silman, I. & Sussman, J. L. (1997). *Theoretical and Computational Methods in Genome Research*, edited by S. Suhai, pp. 303–315. New York: Plenum Press.
Harel, M., Kleywegt, G. J., Ravelli, R. B. G., Silman, I. & Sussman, J. L. (1995). *Structure*, **3**, 1355–1366.
Harel, M., Kryger, G., Rosenberry, T. L., Mallender, W. D., Lewis, T., Fletcher, R. J., Guss, J. M., Silman, I. & Sussman, J. L. (2000). *Protein Sci.* **9**, 1063–1072.
Harel, M., Quinn, D. M., Nair, H. K., Silman, I. & Sussman, J. L. (1996). *J. Am. Chem. Soc.* **118**, 2340–2346.
Harvey, A. L. (1991). *Snake Toxins*. New York: Pergamon.
Hendsch, Z. S., Jonsson, T., Sauer, R. T. & Tidor, B. (1996). *Biochemistry*, **35**, 7621–7625.
Hosea, N., A., Radic, Z., Tsigelny, I., Berman, H. A., Quinn, D. M. & Taylor, P. (1996). *Biochemistry*, **35**, 10995–11004.
Karlsson, E., Mbugua, P. M. & Rodriguez-Itthurralde, D. (1984). *J. Physiol. (Paris)*, **79**, 232–240.
Koellner, G., Kryger, G., Millard, C. B., Silman, I., Sussman, J. L. & Steiner, T. (2000). *J. Mol. Biol.* **296**, 713–735.
Kraut, D., Goff, H., Pai, R. K., Hosea, N. A., Silman, I., Sussman, J. L., Taylor, P. & Voet, J. G. (2000). *Mol. Pharmacol.* **57**, 1243–1248.
Kronman, C., Velan, B., Gozes, Y., Leitner, M., Flashner, Y., Lazar, A., Marcus, D., Sery, T., Papier, Y., Grosfeld, H., Cohen, S. & Shafferman, A. (1992). *Gene*, **121**, 295–304.
Kryger, G., Silman, I. & Sussman, J. L. (1999). *Structure*, **7**, 297–307.
Malany, S., Sawai, M., Sikorski, R. S., Seravalli, J., Quinn, D. M., Radic, Z., Taylor, P., Kronman, C., Velan, B. & Shafferman, A. (2000). *J. Am. Chem. Soc.* **122**, 2981–2987.
Marchot, P., Ravelli, R. B. G., Raves, M. L., Bourne, Y., Vellom, D. C., Kanter, J., Camp, S., Sussman, J. L. & Taylor, P. (1996). *Protein Sci.* **5**, 672–679.

Masson, P., Fortier, P. L., Alnaret, C., Froment, M. T., Bartels, C. F. & Lockridge, O. (1997). *Biochem. J.* **327**, 601–607.
Massoulié, J., Pezzementi, L., Bon, S., Krejci, E. & Vallette, F.-M. (1993). *Prog. Neurobiol.* **14**, 31–91.
Massoulié, J., Sussman, J. L., Doctor, B. P., Soreq, H., Velan, B., Cygler, M., Rotundo, R., Shafferman, A., Silman, I. & Taylor, P. (1992). *Multidisciplinary Approaches to Cholinesterase Functions*, edited by A. Shafferman & B. Velan, pp. 285–288. New York: Plenum Press.
Millard, C. B. & Broomfield, C. A. (1995). *J. Neurochem.* **64**, 1909–1918.
Millard, C. B., Koellner, G., Ordentlich, A., Shafferman, A., Silman, I. & Sussman, J. L. (1999). *J. Am. Chem. Soc.* **121**, 9883–9884.
Navaza, J. (1994). *Acta Cryst.* A**50**, 157–163.
Ordentlich, A., Barak, D., Kronman, C., Ariel, N., Segall, Y., Velan, B. & Shafferman, A. (1996). *J. Biol. Chem.* **271**, 11953–11962.
Ordentlich, A., Barak, D., Kronman, C., Benschop, H. P., De Jong, L. P. A., Ariel, N., Barak, R., Segall, Y., Velan, B. & Shafferman, A. (1999). *Biochemistry*, **38**, 3055–3066.
Ordentlich, A., Kronman, C., Barak, D., Stein, D., Ariel, N., Marcus, D., Velan, B. & Shafferman, A. (1993). *FEBS Lett.* **334**, 215–220.
Rachinsky, T. L., Camp, S., Li, Y., Ekström, J., Newton, M. & Taylor, P. (1990). *Neuron*, **5**, 317–327.
Radic, Z., Durán, R., Vellom, D. C., Li, Y., Cerveñansky, C. & Taylor, P. (1994). *J. Biol. Chem.* **269**, 11233–11239.
Radic, Z., Gibney, G., Kawamoto, S., MacPhee-Quigley, K., Bongiorno, C. & Taylor, P. (1992). *Biochemistry*, **31**, 9760–9767.
Saxena, A., Doctor, B. P., Maxwell, D. M., Lenz, D. E., Radic, Z. & Taylor, P. (1993). *Biochem. Biophys. Res. Commun.* **197**, 343–349.
Saxena, A., Viragh, C., Frazier, D. S., Kovach, I. M., Maxwell, D. M., Lockridge, O. & Doctor, B. P. (1998). *Biochemistry*, **37**, 15086–15096.
Schumacher, M., Camp, S., Maulet, Y., Newton, M., MacPhee-Quigley, K., Taylor, S. S., Friedmann, T. & Taylor, P. (1986). *Nature (London)*, **319**, 407–409.
Shafferman, A., Kronman, C., Flashner, Y., Leitner, M., Grosfeld, H., Ordentlich, A., Gozes, Y., Cohen, S., Ariel, N., Barak, D., Harel, M., Silman, I., Sussman, J. L. & Velan, B. (1992). *J. Biol. Chem.* **267**, 17640–17648.
Shafferman, A., Ordentlich, A., Barak, D., Kronman, C., Ariel, N., Leitner, M., Segall, Y., Blomberg, A., Reuveny, S., Marcus, D., Bino, T., Lazar, A., Cohen, S. & Velan, B. (1995). *Enzymes of the Cholinesterase Family*, edited by A. L. Balasubramanian, B. P. Doctor, P. Taylor & D. M. Quinn, pp. 189–196. New York: Plenum Press.
Shafferman, A., Ordentlich, A., Barak, D., Kronman, C., Ariel, N. & Velan, B. (1998). *Structure and Function of Cholinesterases and Related Proteins*, edited by B. P. Doctor, P. Taylor, D. M. Quinn, R. L. Rotundo & M. K. Gentry, pp. 203–209. New York: Plenum Press.
Shafferman, A., Ordentlich, A., Barak, D., Kronman, C., Grosfeld, H., Stein, D., Ariel, N., Segall, Y. & Velan, B. (1996). *Phosphorus Sulfur Silicon*, **109–110**, 393–396.
Shafferman, A., Ordentlich, A., Barak, D., Stein, D., Ariel, N. & Velan, B. (1996). *Biochem. J.* **318**, 833–840.
Shafferman, A., Velan, B., Ordentlich, A., Kronman, C., Grosfeld, H., Leitner, M., Flashner, Y., Cohen, S., Barak, D. & Ariel, N. (1992). *EMBO J.* **11**, 3561–3568.
Silman, I. & Sussman, J. L. (2000). *Cholinesterases and Cholinesterase Inhibitors*, edited by E. Giacobini, pp. 9–25. London: Martin Dunitz.
Soreq, H., Ben-Aziz, R., Prody, C. A., Seidman, S., Gnatt, A., Neville, L., Lieman-Hurwitz, J., Lev-Lehman, E., Ginzberg, D., Lapidot-Lifson, Y. & Zakut, H. (1990). *Proc. Natl Acad. Sci. USA*, **87**, 9688–9692.
Sussman, J. L., Harel, M., Frolow, F., Oefner, C., Goldman, A., Toker, L. & Silman, I. (1991). *Science*, **253**, 872–879.
Sussman, J. L., Harel, M., Frolow, F., Varon, L., Toker, L., Futerman, A. H. & Silman, I. (1988). *J. Mol. Biol.* **203**, 821–823.
Thompson, J. D., Gibson, T. J., Plewniak, F., Jeanmougin, F. & Higgins, D. G. (1997). *Nucleic Acids Res.* **25**, 4876–4882.
Velan, B., Grosfeld, H., Kronman, C., Leitner, M., Gozes, Y., Lazar, A., Flashner, Y., Marcus, D., Cohen, S. & Shafferman, A. (1991). *J. Biol. Chem.* **266**, 23977–23984.
Velan, B., Kronman, C., Ordentlich, A., Flashner, Y., Leitner, M., Cohen, S. & Shafferman, A. (1993). *Biochem. J.* **296**, 649–656.
Weinstock, M. (1995). *Neurodegeneration*, **4**, 349–356.